Clays and Clay Minerals, Vol. 57, No. 4, 416–424, 2009.

TERAHERTZ TIME-DOMAIN SPECTROSCOPY OF SELECTED LAYERED SILICATES

MARIÁN JANEK[1,2,*], IGNÁC BUGÁR[3], DUŠAN LORENC[3,4], VOJTECH SZÖCS[5], DUŠAN VELIČ[2,3], AND DUŠAN CHORVÁT[3]

[1] Institute of Technology, Slovak Academy of Sciences, Dúbravská cesta 9, SK-84513 Bratislava, Slovakia
[2] Comenius University, Faculty of Natural Sciences, Department of Physical and Theoretical Chemistry, Mlynská dolina CH1, SK-84215 Bratislava, Slovakia
[3] International Laser Centre, Ilkovicova 3, SK-81219 Bratislava, Slovakia
[4] TU Vienna, Institut für Photonik, Gusshausstrasse 27/387, A-1040 Wien, Austria
[5] Comenius University, Faculty of Natural Sciences, Institute of Chemistry, Mlynská dolina CH2, SK-84215 Bratislava, Slovakia

Abstract—Micaceous layer silicate clay minerals are attractive materials for applications involving nonlinear optics because of their low cost and ability to form well ordered, platy aggregates, but such applications require precise knowledge of the dielectric behavior of the clay. The purpose of the present study was to use Terahertz time-domain spectroscopy (THz-TDS) to determine the dielectric properties of certain cleavable layered clay minerals, including muscovite, vermiculite, phlogopite, and biotite. The samples were characterized by X-ray diffraction and Fourier transform infrared spectroscopy as well as chemical analysis by Energy dispersive X-ray spectroscopy. The THz frequency window investigated was the far-infrared region of 3.3 to ~40.0 cm^{-1} corresponding to 0.1 and 1.2 THz, respectively. The samples were selected so that the hydrated form of the interlayer cation, *e.g.* Mg^{2+} present in the interlayer gallery of vermiculite, could be compared to species such as phlogopite, biotite, and muscovite with the dehydrated form of interlayer cations such as K^+ or Na^+. The frequency-dependent complex index of refraction of these natural materials was determined to vary between 2.50 and 2.80. The presence of water in the interlayer space of vermiculite was reflected in the detection of increased values of the absorption index in comparison with the muscovite, phlogopite, and biotite.

Key Words—Absorption Index, Biotite, Far-infrared, Index of Refraction, Layered Silicates, Muscovite, Phlogopite, THz-TDS, Vermiculite.

INTRODUCTION

Terahertz time-domain spectroscopy (THz-TDS) covers the far-infrared (far-IR) frequency region including 0.1−10 THz. Recent developments of this unique spectroscopic technique have included its application in the characterization of semiconductors and dielectric materials (Grischkowsky *et al*., 1990; Labbé-Lavigne *et al*., 1998; Mickan *et al*., 2002; Lee *et al*., 2003; Dai *et al*., 2004), in medicine and biomolecular systems (Fischer *et al*., 2002; Walther *et al*., 2003; Fischer *et al*., 2005a, 2005b; Takahashi *et al*., 2005, 2006; Kröll *et al*., 2006), and to glass and/or non-crystalline solids (McIntosh *et al*., 1997; Naftaly and Miles, 2005; Kojima *et al*., 2005). Further applications of THz-TDS are in defense against terrorism, tomographic imaging, material-quality checking, and chemical sensing. The main advantage of this technique is that the transmitted THz electric field is measured coherently, which provides both high sensitivity and time-resolved phase information and thus promises rich spectroscopic image analysis (Ferguson and Zhang, 2002).

Han *et al*. (2001) published a comparison of both far-IR spectroscopic techniques: terahertz time-domain and far-infrared Fourier transform spectroscopy (far-FTIR). These authors concluded that far-FTIR spectroscopy in general is better than THz-TDS if the frequency is over 5 THz (>167 cm^{-1}); however, at lower frequencies, *e.g.* <3 THz (<100 cm^{-1}), the THz-TDS has much better signal to noise ratio than far-FTIR. Additionally, the time-gated and coherent nature of THz-TDS makes this method suitable for other specific applications (Han *et al*., 2001).

To date, the only report of the application of this technique to the investigation of clay minerals was by Nagai *et al*. (2004). Those authors investigated the dielectric properties of clay-based polyamide nanocomposite films. Their findings clearly showed that an imaginary part of the dielectric constant in the investigated frequency range had been increased significantly in comparison to pure polyamide or a polyamide microcomposite. Further analysis of the results by means of a Debye relaxation formula indicated effective change of molecular interaction and relaxation time of polymer functional groups with the montmorillonite

* E-mail address of corresponding author:
Marian.Janek@savba.sk

This paper, presented during mid-European Clay Conference, held in Zakopane, Poland, during September 2008, is dedicated to Prof. Gerhard Lagaly on the occasion of his 70th birthday

DOI: 10.1346/CCMN.2009.0570402

surface, at low silicate contents (1 w/w%) in the prepared nanocomposite.

THz-TDS is able to extract from one sample measurement, including the determination of a background spectrum, the frequency dependence of the complex refractive index ($\tilde{n}_s = n_s - i\kappa_s$) (Sharma, 2006) of the investigated material (the real part of the refractive index, n_s, and the absorption index, κ_s, as the imaginary part) and, at the same time, the thickness, l, of the absorbing medium (Duvillaret *et al*., 1996). For this purpose, sophisticated numerical algorithms were proposed by Duvillaret *et al*. (1996) and Dorney *et al*. (2001). Withayachumnankul *et al*. (2005a, 2005b) proposed a stable, fast-convergent method for material-parameter extraction using THz-TDS and called it the fixed-point iteration method. The same calculation method was applied in the present study.

Due to their low cost, micaceous layer silicate clay minerals may be attractive materials for optical applications, such as terahertz and non-linear optics, but these applications require an exact knowledge of both the index of refraction and absorption coefficient of the clay. Characterization of these properties of such natural materials by THz-TDS in the far-infrared region is promising, but challenging because the dielectric properties are generally frequency dependent (Hollas, 2004). Results presented here demonstrate, for the first time, how THz-TDS can be used to overcome this difficulty in order to characterize the dielectric properties of several micaceous clay minerals, including muscovite, vermiculite, phlogopite, and biotite. These sample selections were made on the basis of differences in their crystallochemical composition and ability to form well ordered platy crystals suitable for measurement by THz-TDS.

EXPERIMENTAL

Materials

A Spanish vermiculite from the Santa-Olalla deposit, Huelva; a Russian phlogopite from Kovborsk at Bajkal see; a Norwegian muscovite; and a Norwegian biotite from Vådme-Iveland were used in this study. A small amount of each sample was crushed in an agate mortar and used for X-ray diffraction (XRD) and Fourier transform infrared (FTIR) analyses. Both techniques confirmed that the samples represented almost pure mineralogical species of layered minerals, except for the muscovite in which a calcite impurity was detected. The mean elemental ratios giving the chemical compositions were achieved by energy dispersive X-ray spectroscopy (EDS) (Table 2). A platy fragment of the sample ~0.3–0.5 mm thick was separated, using a scalpel, from the raw material, and used directly for THz-TDS measurements.

Techniques

X-ray diffraction patterns from the powdered muscovite, vermiculite, phlogopite, and biotite materials were obtained using a Stoe Stadi-P transmission X-ray powder diffractometer equipped with a curved Ge(111) primary beam monochromator and Co radiation (CoKα_1, λ = 0.178896 nm). The patterns were scanned in the range 3–75º2θ with a step size of 0.02º2θ and 1.5 s/step.

Infrared spectra of the powdered materials were obtained using a KBr pressed-disc technique on a Nicolet Magna 750 FTIR spectrometer equipped with a DTGS detector. Spectra were recorded over the range 4000–400 cm^{-1}, accumulating 32 spectral scans, with a resolution of 4 cm^{-1}. A background signal was collected prior to each scan. The first spectrum of each sample investigated was collected from KBr disks dried at 110ºC for a period of 24 h and the further spectra were collected in an atmosphere from which water vapor was removed. The spectra were evaluated using the data-collection and control software *Omnic*® (Thermo Electron Corporation).

Energy dispersive X-ray spectroscopy (EDS) was performed using an EVO 40 electron microscope (Karl-Zeiss Jena, Germany) to obtain the mean elemental compositions of the samples analyzed. A piece of sample was stuck to a conventional sample holder and covered with gold in a commercial sputtering unit. The sample and holder were then transferred to the microscope chamber and EDS measurements of the elemental ratios performed at magnifications of 100× from areas of ~0.5 mm^2. The mean values from at least five different points on the sample surfaces were calculated.

The THz-TDS measurements were performed using a device constructed in the International Laser Center, Bratislava, and based on a femtosecond-laser-driven photoconductive emitter and antenna detector (Figure 1). The THz emitter and detector were supplied by the International Laser Center of Lomonosov University (Moscow, Russia). Laser pulses were generated by a Ti:sapphire oscillator (CDP TiF50, Moscow, Russia) providing pulses ~80 fs long. The Ti:sapphire oscillator was driven by a Coherent Verdi 5W device at a wavelength of 532 nm. The THz emitter was irradiated with 12 mW of power and the detector with 7 mW of power at a central pulse wavelength of ~800 nm. The emitter, based on low-T GaAs with surface Au metallic stripes, was biased at 18 V and symmetrically modulated at 15 kHz. The THz polarization is linear for the photo-optical switches as the electric field on the emitter is directed from one electrode to another (Reimann, 2007). Varying the position of the delay line led to a time delay of the probe beam arriving on the emitter and detector, resulting in a measurement of the electric-field dependence of the THz pulse directly in the time domain (using a lock-in amplifier, Model SR830 DSP, Stanford Research Systems, USA). All measurements were performed at the air-conditioned temperature of the laboratory equal to 21.0±1.0ºC.

During measurements, the platy clay sample was inserted perpendicular to the THz beam, hence the

https://doi.org/10.1346/CCMN.2009.0570402 Published online by Cambridge University Press

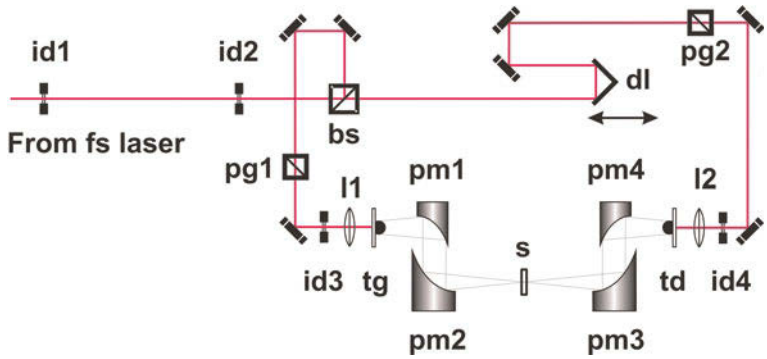

Figure 1. Scheme of the THz-TDS setup based on femtosecond-laser driven photoconductive emitter and antenna detector (id – iris diaphragm, bs – beam splitter, pg – Glan prism, pm – parabolic mirror, l – lens, dl – delay line, tg – terahertz generator, td – terahertz detector, s – sample).

incidence was normal to the *ab* plane of silicate layers. To minimize the effects of possible anisotropic properties of selected clay species known from optical crystallograpy (Wahlstrom, 1960), replica measurements on two different sample orientations, with an arbitrary angle of 90º around the *c* axes, were used to achieve the mean values of frequency-dependent complex index of refraction ($\tilde{n}_s = n_s - i\kappa_s$). In order to extract the material parameters, the fixed-point iteration method suggested by Withayachumnankul *et al*. (2005a, 2005b) was used.

RESULTS AND DISCUSSION

Characteristics of cleavable layered clay minerals

The XRD patterns showed typical patterns for dioctahedral (muscovite) and trioctahedral (vermiculite, phlogopite, and biotite) clay minerals investigated in our study (Figure 2). Muscovite (like phlogopite and biotite) revealed the first basal reflection at ~1.00 nm indicating that these micas are composed of fully collapsed layers with no available interlayer space. On the contrary, the vermiculite shows the first basal reflection at 1.44 nm indicating that hydrated cations are present in the interlayer space, providing a gallery height of 0.44 nm. Phlogopite and biotite have almost identical XRD patterns, but, as demonstrated by the IR spectra (Figure 3) and by the EDS results, the chemical compositions of these species differ significantly; reflected also by differences in the absorption bands of the OH-stretching and bending region (Farmer, 1974).

The phlogopite used in the present study contained much less structural Fe than did the biotite, the latter which revealed the presence of stretching bands corresponding to Mg_2FeOH and MgFeOH, and the deformation band of MgFeOH (3594, 3562, and 762 cm^{-1}) (Figure 3, Table 1). Interestingly, based on

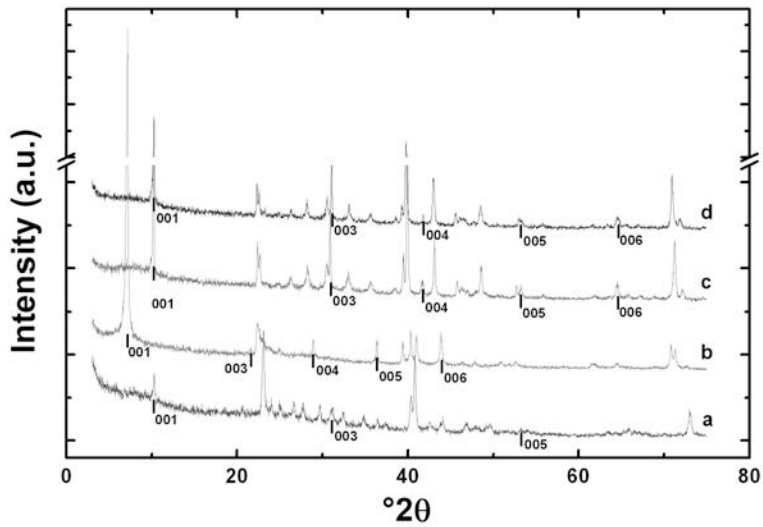

Figure 2. XRD patterns of the samples: a – muscovite, b – vermiculite, c – phlogopite, d – biotite; the 00*l* diffractions are indicated directly under corresponding peaks.

https://doi.org/10.1346/CCMN.2009.0570402 Published online by Cambridge University Press

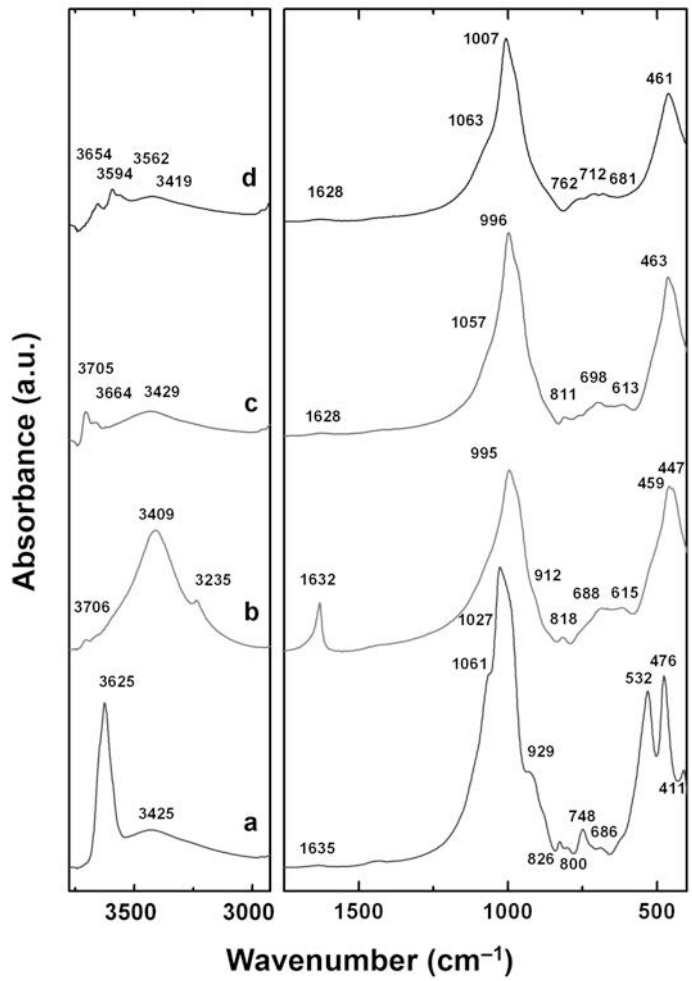

Figure 3. FTIR patterns of the investigated samples: a – muscovite, b – vermiculite, c – phlogopite, d – biotite.

comparison of the IR absorption bands for phlogopite and vermiculite, the structural composition of phlogopite should be expected to be very close to that of vermiculite. However, the significant difference is in the presence of hydrated cations in the interlayer galleries of vermiculite. A typical water vibration stretching band at 3409 cm^{-1} and a deformation band at 1632 cm^{-1} were detected in the IR spectra of vermiculite. Assignments of the absorption bands are summarized in Table 1. Predictions of the differences in the chemical composition based on IR spectroscopy were also confirmed by the EDS analyses (Table 2). The chemical composition of vermiculite layers, as the Mg-rich variety having hydrated Mg^{2+} cations in the interlayer galleries, is rather similar to the composition of phlogopite. Muscovite as the Al-rich variety of mica has significant K^+ alongside the Na^+ in the interlayer galleries, similar to the phlogopite and biotite samples. The biotite had four times as much structural Fe as phlogopite (Table 2).

Dielectric properties of layered silicates in the THz region

Averaged THz impulses from at least three experimental replicas of the silicon wafer used as a material standard with known refractive properties were also evaluated (data not shown). The main impulse peak observed in a nitrogen atmosphere at 8.35 ps had full width at half maximum for the positive half-cycle of ~0.73 ps and was also observable for the silicon sample. However, the impulse position shifted to a higher delay value of 12.54 ps and the intensity decreased. The sample pattern displayed low-intensity impulses that are the time-domain analogue to the Fabry-Perot effect related to multiple internal reflections at 24.34, 36.04, and 47.83 ps (Duvillaret, 1996). Delay of the main impulse peak is related to both the magnitude of the refractive index n_{Si} as well as the thickness of the sample. The decrease in the peak intensity is similarly affected by the magnitude of absorption index κ_{Si} and the sample thickness. The Fabry-Perot reflections

https://doi.org/10.1346/CCMN.2009.0570402 Published online by Cambridge University Press

Table 1. Attribution of IR absorption bands.

Wavenumber (cm^{-1})	Attribution
3405−3430	OH stretching vibrations of water
1628−1635	OH deformation vibrations of water
Muscovite	
3625	Al_2-OH stretching
1435	calcite admixture ($CaCO_3$)
1061	Si-O_{ap} stretching (ap = apical)
1027	Si−O stretching (in-plane)
929	Al_2-OH deformation
881	calcite admixture ($CaCO_3$)
826	Al−O stretching (Al in tetrahedral sheet)
800	Si−O deformation
748	Al−O−Al stretching (Al in tetrahedral sheet)
686	Si−O deformation
532	Al−O−Si (Al in octahedral sheet)
476	Si−O−Si deformation
411	Si−O−Si deformation
Vermiculite	
3706	Mg_3−OH stretching
3233	overtone of water OH deformation
995	Si−O stretching
818	Al−O stretching (Al in tetrahedral sheet)
688	Si−O deformation
615	Mg_3−OH deformation
459	Si−O−Si deformation
447	Si−O−Si deformation
Phlogopite	
3705	Mg_3−OH stretching
3664	Mg_2Al−OH stretching
1057	Si−O_{ap} stretching
996	Si−O stretching
811	Al−O stretching (Al in tetrahedral sheet)
698	Si−O deformation
613	OH deformation
463	Si−O−Si deformation
Biotite	
3654	Mg_2Al−OH stretching
3594	Mg_2Fe^{3+}−OH stretching
3562	$MgFe^{3+}$−OH stretching
1063	Si−O_{ap} stretching
1007	Si−O stretching
762	MgFe−OH deformation
712	Si−O deformation
681	Mg_3−OH deformation
461	Si−O−Si deformation

inherently include also all of the above-mentioned factors. Applying the numerical algorithms proposed by Withayachumnankul *et al*. (2005a, 2005b), refractive properties of silicon ($\tilde{n}_{Si} = n_{Si} - i\kappa_{Si}$) were calculated. The thickness, l, of the silicon wafer was found by this method to be 0.52 mm, which compared favorably with the thickness of 0.50±0.05 mm measured mechanically with a sliding calliper, indicating that the result achieved from THz-TDS measurement is within the frame of the sliding calliper experimental error.

The dielectric properties of silicon at a frequency of ~1.0 THz are known from published literature ($\tilde{n}_{Si}$ = 3.417 − i0) (Dai, 2004). Results achieved by measurements in the present study were in very good agreement with the literature values, as indicated by mean values of refractive index of n_{Si} = 3.41±0.01 and absorption index of κ_{Si} = 0.01±0.01 at the frequency of 1.0 THz. The absorption index can be within the frame of experimental error considered equal to zero.

At this point, notice that, from the known frequency dependence of the refractive (real part) and absorption (imaginary part) indices and application of Maxwell's relations, the wavenumber dependence of the complex dielectric permitivity of the sample, $\tilde{\varepsilon}_{r,s} = \varepsilon_{1,s} - i\varepsilon_{2,s}$, can be calculated ($\varepsilon_{1,s} = n_s^2\ \kappa_s^2$, $\varepsilon_{2,s} = 2n_s\kappa_s$). The real part of the permitivity, $\varepsilon_{1,s}$, is characteristic of the polarizability of the material as well as of the propagation of the radiation into the material. The loss factor, $\varepsilon_{2,s}$, indicates the ability of the material to dissipate electric energy.

From the selected group of layered clay minerals, micas are usually used as insulators or dielectrics in specific electro-technical applications. The THz-TDS represents a unique technique to investigate the dielectric properties of these layered materials at THz frequencies. Typical THz impulses propagating through the nitrogen atmosphere used as a background medium and through the phlogopite sample are shown in Figure 4a. For some platy materials, e.g. phlogopite and biotite, multiple internal reflections were apparent due to the high degree of alignment of individual layers within these samples. For muscovite and vermiculite, considerable stacking disorder was apparent, as these samples did not show these reflections. The main impulse peak was delayed 2.00 ps for phlogopite compared to the background nitrogen atmosphere (Figure 4a). The corresponding fast Fourier-transform spectra of phlogopite and the background nitrogen atmosphere (Figure 4b), on a frequency scale, indicate that the useful signal level for phlogopite is in the range of ~0.1−1.2 THz. The sample thickness revealed from these measurements was 0.33 mm, which is in good agreement with the sliding calliper measurement of 0.35±0.05 mm.

For the biotite, vermiculite, and muscovite, the impulse positions shifted by 2.10, 3.15, and 1.90 ps (data not shown), respectively, with respect to the nitrogen background, and the thicknesses of the samples measured with the sliding calliper were 0.35±0.05, 0.50±0.05, and 0.35±0.05 mm, respectively. The thickness of biotite determined from the numerical calculations of the THz signal was 0.35 mm. Due to the above-mentioned geometrical imperfections in the muscovite and vermiculite samples, sliding calliper values instead of THz values for sample thickness were used for the calculations of complex refractive index of these materials.

https://doi.org/10.1346/CCMN.2009.0570402 Published online by Cambridge University Press

Table 2. Mean elemental composition of investigated samples as determined by EDS analysis.

Sample	Atomic percent[#] (%)									
	Si	Al	Fe	Mg	Ti	Mn	Ca	Na	K	O
Biotite	14.6 (0.9)	8.1 (0.5)	8.0 (0.7)	4.6 (0.2)	1.0 (0.1)	0.3 (<0.1)	<0.1 (<0.1)	0.1 (0.1)	5.1 (0.5)	58 (2)
Phlogopite	13.3 (0.7)	7.1 (0.4)	2.0 (0.1)	11.2 (0.7)	0.7 (0.1)	n.d.	0.1 (<0.1)	0.5 (0.1)	4.6 (0.3)	60 (2)
Vermiculite	11.4 (1.6)	6.4 (0.8)	1.1 (0.2)	12.9 (1.4)	n.d.	n.d.	0.1 (<0.1)	n.d.	n.d.	68 (4)
Muscovite	16.4 (0.5)	14.4 (0.4)	1.3 (<0.1)	0.5 0.1	0.1 (<0.1)	n.d.	<0.1 (<0.1)	0.5 (0.1)	5.2 (0.1)	62 (1)

[#] – standard deviations in parenthesis; n.d. – not detectable

The frequency dependence of refractive index, n_{sample}, and absorption index, κ_{sample}, of cleavable clay samples (Figure 5) revealed no specific absorption line within the accessible frequency window. At THz frequencies, the electro-magnetic wave propagation in the solid is affected by the presence of localized charges (Schlömann, 1964, Strom and Taylor, 1977). The mean values of refractive indexes differed slightly among the muscovite, phlogopite, and biotite samples and covered the range 2.73, 2.76, and 2.82, respectively, at a frequency of ~1 THz.

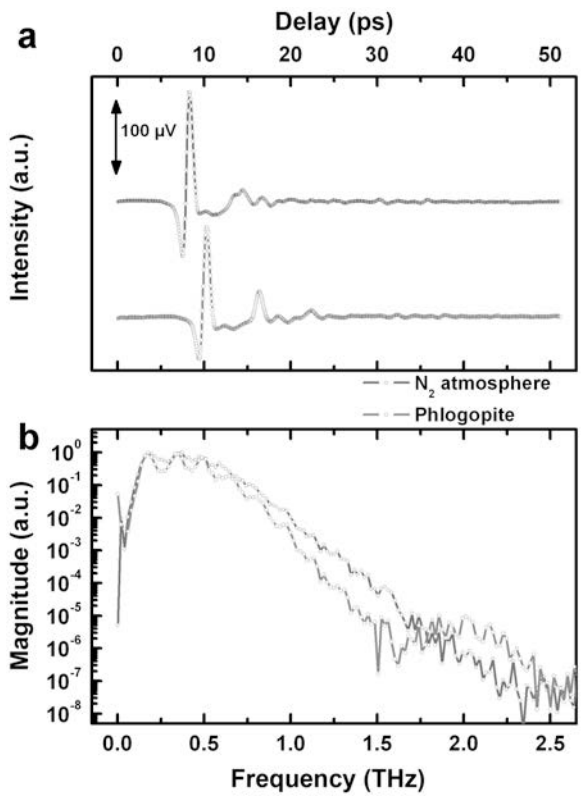

Figure 4. Typical impulses of THz radiation as detected in the nitrogen atmosphere and phlogopite sample in a nitrogen atmosphere – a, spectra of phlogopite and nitrogen atmosphere as background on frequency scale – b.

The mean refractive index of vermiculite, at 2.51, was significantly lower than the other samples. The reason for this is unclear, as the chemical composition of the layers is similar to that of phlogopite. One possible explanation for this phenomenon may be connected to the water content present in the form of hydration water of interlayer magnesium cations of vermiculite. The absorption indexes of muscovite, phlogopite, and biotite were close to zero; however, the absorption index of vermiculite was slightly greater than the above-mentioned samples. Water exhibits a monotonic trend of increasing absorption coefficient with increasing frequency in the far infrared (THz) region (Thrane, 1995, Kindt and Schmuttenmaer, 1996) and the present results revealed a slightly increased absorption index for vermiculite (Figure 5), which could be attributed to this phenomenon of adsorbed water.

Noteworthy is the significant variance calculated for the refractive index of a single sample as it was rotated 90º around the *c* axis while keeping normal beam incidence. These variances were compared (Figure 5) with the angular dependence of the index of refraction as known from optical crystallography (Wahlstrom, 1960, Rieder *et al.*, 1971) and differences were found (Figure 5). This behavior may be related either to the uncertainty of sample thickness determination (muscovite, vermiculite) or to the quality of stacking order of single layers forming the given polytype, resulting in the detection of differences of the isotropic properties (e.g. biotite vs. phlogopite). Nevertheless, this hypothesis will require a more detailed study of refractive properties of polarized incident beam angle and sample orientation.

https://doi.org/10.1346/CCMN.2009.0570402 Published online by Cambridge University Press

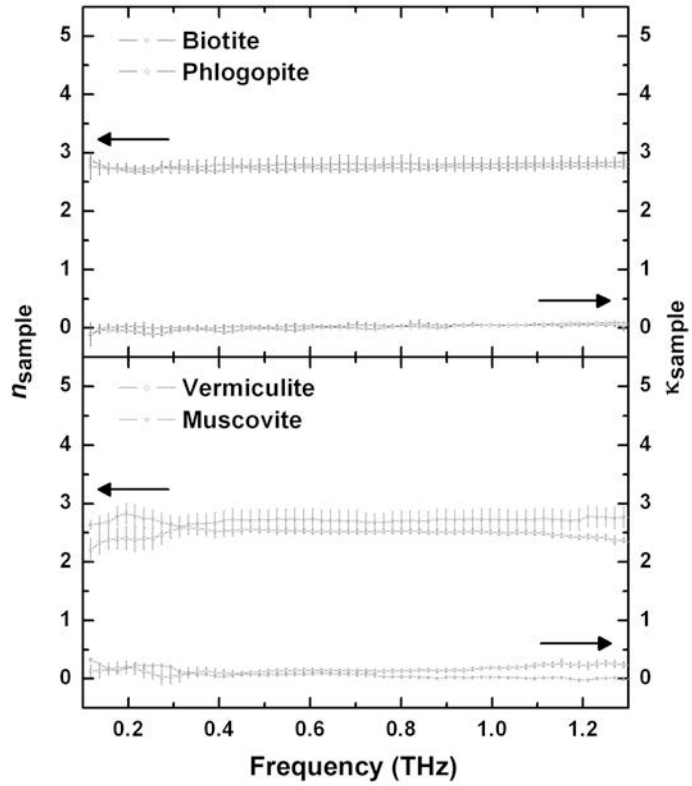

Figure 5. Frequency-dependent refractive n_{sample} and absorption κ_{sample} index of muscovite, vermiculite, phlogopite and biotite samples. The error bars correspond to the standard deviation values of two multiple replicas distinguished by 90º sample rotation with respect to the incident THz probe radiation.

CONCLUSIONS

Terahertz time-domain spectroscopy (THz-TDS) was demonstrated to be a useful method for the determination of the frequency-dependent refractive properties of layered clay minerals such as muscovite, vermiculite, phlogopite, and biotite. For planar, well crystallised species such as phlogopite and biotite the sample thickness was also determined by this method, using the time-domain analogue of the Fabry-Perot effect. This technique easily also delivers through Maxwell's relations the frequency dependence of the complex dielectric permitivity of the material, which is related to the refractive properties.

A significant variation of frequency-dependent complex index of refraction of the selected samples was within the interval 2.50−2.80. Due to the detection of the significantly different values of the variance among the single-sample refractive indexes after the change of incident beam angle and sample orientation, the quality of stacking order of single layers forming a given polytype could play a role in the detected anisotropic properties. However, this hypothesis will require a more detailed study. The presence of water in the interlayer space of vermiculite was reflected in the detection of increased values of absorption index in comparison to the muscovite, phlogopite, and biotite samples.

ACKNOWLEDGMENTS

The assistance of Dr M. Nazarov and Dr D. Sapozhnikov during construction of the THz device (MSU, Moscow), of Mrs A. Jurová (IIC SAS, Bratislava) during EDS measurements, of Mrs I. Macková (IIC SAS, Bratislava) during XRD measurements, and of Mr A. Gaál (ILC, Bratislava) with fs laser operation is acknowledged. Thanks are also extended to Prof. I. Kraus (CU, Bratislava) for providing the muscovite and phlogopite samples, as well as to Prof. G. Lagaly and Mr K. Beneke (CAU, Kiel) for supplying the vermiculite sample. Dr J. Madejová is thanked for her comments on the IR spectroscopic results. The financial support of the Slovak Grant Agency for Science VEGA (grant No. 1/4457/07) is greatly appreciated.

REFERENCES

Dai, J., Zhang, J., Zhang, W., and Grischkowsky D. (2004) Terahertz time-domain spectroscopy characterization of the far-infrared absorption and index of refraction of high-resistivity, float-zone silicon. *Journal of the Optical Society of America*, **B7**, 1379−1386.

Dorney, T.D., Baraniuk, R.G., and Mittelman, D.M. (2001) Material parameter estimation with terahertz time-domain spectroscopy. *Journal of the Optical Society of America A*, **18**, 1562−1571.

Duvillaret, L., Garet, F., and Coutaz, J.L. (1996) A reliable method for extraction of material parameters in terahertz time-domain spectroscopy. *IEEE Journal of Selected Topics*

in Quantum Electronics, **2**, 739–746.
Farmer, V.C. (editor) (1974) *Infrared Spectra of Minerals*. Monograph **4**, Mineralogical Society, London, p. 331.
Ferguson, B. and Zhang, X.C. (2002) Materials for terahertz science and technology. *Nature Materials*, **1**, 26–33.
Fischer, B.M., Walther, M., and Jepsen, P.U. (2002) Far-infrared vibrational modes of DNA components studied by terahertz time-domain spectroscopy. *Physics in Medicine and Biology*, **47**, 3807–3814.
Fischer, B.M., Hoffmann, M., Helm, H., Wilk, R., Rutz, F., Kleine-Ostmann, T., Koch, M., and Jepsen, P.U. (2005a) Terahertz time-domain spectroscopy and imagin of artificial RNA. *Optics Express*, **13**, 5205–5215.
Fischer, B.M., Hoffmann, M., Helm, H., Wilk, R., Modjesch, G., and Jepsen, P.U. (2005b) Chemical recognition in terahertz time-domain spectroscopy and imagin. *Semiconductor Science and Technology*, **20**, S246–S253.
Grischkowsky, D., Kedding, S., van Exter, M., and Fattinger, C. (1990) Far-infrared time domain spectroscopy with terahertz beams of dielectrics and semiconductors. *Journal of the Optical Society of America*, **B7**, 2006–2015.
Han, P.Y., Tani, M., Usami, M., Kono, S., Kersting, R. and Zhang, X.C., (2001) A direct comparison between terahertz time-domain spectroscopy and far-infrared spectroscopy. *Journal of Applied Physics*, **89**, 2357–2359.
Hollas J.M. (2004) *Modern Spectroscopy*. John Wiley & Sons, Inc., Chichester, UK.
Kindt, J.T. and Schmuttenmaer, C.A. (1996) Far-infrared dielectric properties of polar liquids probed by femtosecond terahertz pulse spectroscopy, *Journal of Physical Chemistry*, **100**, 10373–10379.
Kojima, S., Hitahara, H., Nishizawa, S., Yang, Y.S., and Wada Takeda, M. (2005) Terahertz time-domain spectroscopy of low-energy excitations in glasses. *Journal of Molecular Structure*, **744–747**, 243–246.
Kröll, J., Darmo, J., and Unterreiner, K. (2006) Terahertz optical activity of sucrose single-crystals. *Vibrational Spectroscopy*, **43**, 324–329.
Labbé-Lavigne, S., Barret, S., Garet, F., Duvillaret, L., and Coutaz, J.L. (1998) Far-infrared dielectric constant of porous silicon layers measured by terahertz time-domain spectroscopy. *Journal of Applied Physics*. **83**, 6007–6010.
Lee, K.S., Lu, T.M., and Zhang, X.C. (2003) The measurement of the dielectric and optical properties of nano thin films by THz differential time-domain spectroscopy. *Microelectronics Journal*, **34**, 63–69.
McIntosh, C., Toulouse, J., and Tick, P. (1997) The Boson peak in alkali silicate glasses. *Journal of Non-Crystalline Solids*, **222**, 335–341.
Mickan, S.P., Lee, K.S., Lu, T.M., Munch, J., Abbott, D., and Zhang, X.C. (2002) Double modulated differential THz-TDS for thin film dielectric characterization. *Microelectronics Journal*, **33**, 1033–1042.
Naftaly, N. and Miles, R.E. (2005) Terahertz time-domain spectroscopy: A new tool for the study of glasses in the far infrared. *Journal of Non-Crystalline Solids*, **351**, 3341–3346.
Nagai. N., Imai, T., Fukasawa, R., Kato, K., and Yamaguchi, K., (2004) Analysis of the intermolecular interaction of nanocomposites by THz spectroscopy. *Applied Physics Letters*, **85**, 4010–4012.
Reimann, K. (2007) Table-top sources of ultrashort THz pulses. *Reports on Progress in Physics* **70**, 1597–1632.
Rieder, M., Píchová, A., Fassová, M., Feiduková, E., and Černý P. (1971) Chemical composition and physical properties of lithium-iron micas from the Krušné Hory (Erzgebirge), Czechoslovakia and Germany. Part B: Cell parameters and optical data. *Mineralogical Magazine*, **38**, 190–196.
Schlömann, E. (1964) Dielectric losses in ionic crystals with disordered charge distributions, *Physical Review*, **135**, A413–A419.
Sharma, K.K. (2006) *Optics – Principles and Applications* (K.K. Sharma, editor). Elsevier, Oxford, UK.
Strom, U. and Taylor, P.C. (1977) Temperature and frequency dependence of the far infra-red and microwave optical absorption in amorphous materials, *Physical Review* B, **16**, 5512–5522.
Takahashi, M., Ishikawa, Y., Nishizawa, J., and Ito, H. (2005) Low-frequency vibrational modes of riboflavin and related compounds. *Chemical Physics Letters*, **401**, 475–482.
Takahashi, M., Kawazoe, Y., Ishikawa, Y., and Ito, H. (2006) Low-frequency vibrations of crystalline trehalose dihydrate. *Chemical Physics Letters*, **429**, 371–377.
Thrane. L., Jacobsen, R.H., Uhd Jepsen, P., and Keiding, S.R. (1995) THz reflection spectroscopy of liquid water. *Chemical Physics Letters*, **240**, 330–333.
Wahlstrom, E.E., (1960) *Optical Crystallography*. John Wiley & Sons, Inc., New York.
Walther, M., Fischer, B.M., and Jepsen, P.U. (2003) Noncovalent intermolecular forces in polycrystalline and amorphous saccharides in the far infrared. *Chemical Physics*, **288**, 261–268.
Whitayachumnankul, W., Ferguson, B., Rainsford, T., Mickan, S.P., and Abbott, D. (2005a) Material parameter extraction for terahertz time-domain spectroscopy using fixed-point iteration. Pp. 221–231 in: *Photonic Materials, Devices, and Applications* (G. Badenes, D. Abbott and A. Serpengützel, editors). *Proceedings of the SPIE*, **5840**, Bellingham, Washington, USA.
Whitayachumnankul, W., Ferguson, B., Rainsford, T., Mickan, S.P., and Abbott, D. (2005b) Simple material parameter estimation via terahertz time-domain spectroscopy. *Electronics Letters*, **41**, 800–801.

(*Received 2 December 2008; revised 18 February 2009; Ms. 0243; A.E. D.C. Bain*)

APPENDIX

Numerical treatment of the experimental data was done on the fixed-point iteration method published by Withayachumnankul *et al.* (2005a, 2005b). The method is based on the extraction of the sample (homogeneous material) complex refractive index, $\tilde{n}_{\text{sample}} = n_s - i\kappa_s$, where n_s is a real refractive index and κ_s absorption index.

If a plane wave electric field $E(\omega)$ emitted by the antenna generator is travelling in a free air and impinges at normal incidence (perpendicular to a surface of the material) on a homogeneous material, then the received (transmitted) electromagnetic wave can be expressed by:

$$E_{\text{sample}}(\omega) = \eta\ t_{\text{air, sample}}\ p_{\text{sample}}(\omega,l)\ FP(\omega)\ t_{\text{sample, air}}\ E(\omega) \tag{1}$$

Here, η is the transmission coefficient of free air, $t_{\text{air, sample}}$ ($t_{\text{sample, air}}$) is the transmission coefficient at the air-sample (sample-air) interface and $p_{\text{sample}}(\omega,l) = \exp[-i\tilde{n}_{\text{sample}}\omega l/c]$ is the attenuation factor in the medium over distance l. Further, c is the velocity of the light and $FP(\omega)$ represents the Fabry-Pérot effect, *i.e.* multiple internal reflections within the material:

$$FP(\omega) = \sum_{k=0}^{+\infty}\left\{r_{\text{sample,air}}^2 p_{\text{sample}}^2(\omega,l)\right\}^k = \frac{1}{1-\left(\frac{\tilde{n}_{\text{sample}}-\tilde{n}_{\text{air}}}{\tilde{n}_{\text{sample}}+\tilde{n}_{\text{air}}}\right)^2 \exp\left[-2i\tilde{n}_{\text{sample}}\frac{\omega l}{c}\right]} \tag{2}$$

where $r_{\text{sample,air}}$ is the reflection coefficient at the sample-air interface.

In the case that the plane wave travels an identical path without the presence of the sample, the description of electric field of reference wave is given by:

$$E_{\text{ref}}(\omega) = \eta\, p_{\text{air}}(\omega,l)\, E(\omega) \tag{3}$$

A transfer function $H(\omega)$ of the sample is obtained by deconvolving the received spectrum with respect to the reference spectrum:

$$H_{\text{measured}}(\omega) = \frac{E_{\text{sample}}(\omega)}{E_{\text{ref}}(\omega)} = \frac{4\tilde{n}_{\text{sample}}\cdot\tilde{n}_{\text{air}}}{(\tilde{n}_{\text{sample}}+\tilde{n}_{\text{air}})^2}\exp\left[-i(\tilde{n}_{\text{sample}}-\tilde{n}_{\text{air}})\frac{\omega l}{c}\right]\cdot FP(\omega) \tag{4}$$

In the case that the Fabry-Pérot reflections may be eliminated ($FP(\omega) \rightarrow 1$), equation 3 can be rearranged into a complex equation:

$$\arg[H_{\text{measured}}(\omega)] = \arg\left[\frac{4\tilde{n}_{\text{sample}}\cdot\tilde{n}_{\text{air}}}{(\tilde{n}_{\text{sample}}+\tilde{n}_{\text{air}})^2}\right] - (\tilde{n}_{\text{sample}}-\tilde{n}_{\text{air}})\frac{\omega l}{c} \tag{5}$$

this gives for n_s

$$\tilde{n}_{\text{sample}} = g_1(n_s,\kappa_s) = -\frac{c}{\omega l}\left\{\arg[H_{\text{measured}}(\omega)] - \arg\left[\frac{4\tilde{n}_{\text{sample}}\cdot\tilde{n}_{\text{air}}}{(\tilde{n}_{\text{sample}}+\tilde{n}_{\text{air}})^2}\right]\right\} \tag{6}$$

and for κ_s

$$\kappa_{\text{sample}} = g_2(n_s,\kappa_s) = -\frac{c}{\omega l}\left\{\ln[H_{\text{measured}}(\omega)] - \ln\left[\frac{4\tilde{n}_{\text{sample}}\cdot\tilde{n}_{\text{air}}}{(\tilde{n}_{\text{sample}}+\tilde{n}_{\text{air}})^2}\right]\right\} \tag{7}$$

Equations 6 and 7 are in the form suitable for a two dimensional fixed-point iteration, $[n_s,\kappa_s] = f[g_1(n_s,\kappa_s), g_2(n_s,\kappa_s)]$. The initial values of n_s and κ_s maps these points to new points. Repeated substitution of the new values of n_s and κ_s into both equations gives updated values, which according Withayachumnankul *et al.* (2005a, 2005b), converges to desired values.

Finally, the Fabry-Pérot cancelation was incorporated into the recursive process, when the updated transfer function $H(\omega)/FP(\omega)$ is used with mapped values of n_s and κ_s. To eliminate the 'waving' of the frequency dependence of optical parameters, a further step was taken. In fact, the sample length l is known with some accuracy and the theory does not include possible non-parallelness of the sample surfaces. To correct this, the above equations were calculated for a set of different sample lengths, when for each length the frequency 'waving' of optical parameters, *i.e.* absolute value of frequency differences for each n_s and κ_s, were calculated. The result with minimal 'waving' gave the correct value of optical parameters (and the sample length).

https://doi.org/10.1346/CCMN.2009.0570402 Published online by Cambridge University Press